International Journal of Mechanical and Production Engineering Research and Development (IJMPERD)
ISSN (P): 2249–6890; ISSN (E): 2249–8001
Vol. 9, Issue 5, Oct 2019, 287–304

TRANS STELLAR
•Journal Publications • Research Consultancy

DAMPING IMPROVEMENT OF A CANTILEVER BEAM USING TWO PATCHES OF FLUIDIC FLEXIBLE MATRIX COMPOSITE TUBES

SHIREN O. MUHAMMAD & NAZHAD A. HUSSAIN

Department of Mechanical and Mechatronics Engineering, Salahaddin University - Erbil, Iraq

ABSTRACT

Fluidic Flexible Matrix Composite (F^2MC) tubes are promising fiber reinforced tubes, they can passively provide damping and vibration absorption. This study focuses on analyzing F^2MC tube's response to add damping to cantilever structures. A novel cantilever beam vibration absorber encompassing different models of a patch of F^2MC tubes has been examined. A new mathematical model was performed for a system that composed of two short patches instead of one, bonded in various positions on the beam. The study extracted transfer functions of reduced mathematical models of the beam into MATLAB® software. It focused on the amplitude and frequency of resonance of mode shapes. The results demonstrated that F^2MC tubes that composed of two layers of composite fiber reinforced layers from inside reduced the first mode amplitude by 12.12dB. Whereas, increasing the number of patches reduced the first resonance amplitude by 11.12dB. Through comparing the integration of two patches with one patch, single tube is more powerful than a couple of tubes, it gains a reduction of 14dB in First mode shape amplitude. Depending on the above results the study utilized a reduction in both amplitude and frequency of resonance by 20.7dB and 53Hz in FRF plot, respectively.

KEYWORDS: *Vibration Absorbers, F^2MC Tubes, Fiber Reinforced Layers, Frequency Response Function, Mathematical Model & Cantilever Beam*

Received: Jun 18, 2019; **Accepted**: Jul 12, 2019; **Published**: Sep 11, 2019; **Paper Id.**: IJMPERDOCT201925

Original Article

1. INTRODUCTION

Fluidic Flexible Matrix Composite (F^2MC) tubes are a new class of tight, compromise smart and light weight fiber reinforced composite laminates with high degree of anisotropy. The fibers oriented as $\pm\alpha^\circ$ with respect to the longitudinal axis, the layers enclosed a working fluid. The fluid flow is controlled by valve and accumulator. These devices are new candidates of vibration reducers and they can passively provide damping, vibration absorption, and vibration isolation of the structures that directly connected with them.

The first idea of using FMC tubes was found by (Philen, Ying, Bakis, Wang, & Rahn 2006). The authors took advantage from the FMC tube's fiber reinforcement configuration and bulk modulus of working fluid in closed valve scenario to obtain a variable stiffness adaptive smart structure that can be used as energy absorbers. In another study, Ying et al. investigated the capacity of F^2MC tubes for self-governing structural tailoring (Ying Shan et al., 2009). They developed an analytical model to study the axial stiffness of a single F^2MC tube. Some mechanical properties had been tailored, such as: inner liner modulus of elasticity, F^2MC tube's thickness and working fluid's bulk modulus. As a result, a flexible FMC tube with a wider range of tailor ability had been obtained. Also, (Philen, 2010) investigated on an active valve control for tuning the modulus of F^2MC tubes. They derived a simple model for finding the dynamic response of combined system including composite tubes, control valves, and fluid flow rate inside them through experimental tests, with

achievements in reliability of these tubes. Undesired noise and vibrations have a destructive effect in many areas. So, the control of vibrations has become appropriate technological objection. Dynamic Vibration Absorbers (DVAs) are mechanical or electrical systems that can be attached to another mechanical structure or main system for the purpose of controlling vibrations of that system. (Lotfi-Gaskarimahalle, Lioyd H. Scarborough, Christopher D. Rahn, & Edward C. Smith, 2009) studied the efficiency of F^2MC tubes as TVAs which the examined prototype was consisting of two layered F^2MC tube, filled with air. The studied parameters were Fluid inheritance port, orifice size, F^2MC mass system. Their results improved up to a 94% in forced vibration response using these tubes. (Kirn, Lorkowski Thomas, & Baier Horst, 2011) focused on material combinations of F^2MC tubes and their production methods to develop fluidic actuators (flexible in one dimension and stiff in others) in morphing systems. In their study, the authors showed the production capability of easy to use composite materials, and tested the manufactured specimens by tensile test.

(Bin Zhu, Krott, Rahn, & Bakis, 2014) characterized F^2MC tubes experimentally for vibration treatment in cantilever beams by using a patch of a pair of F^2MC tubes. Comparisons had been made between two different fluidic circuits. The first fluidic circuit used orifice for energy dissipation whereas the second used inertia truck and accumulator. Their results showed a reduction in amplitude of vibration in the first mode shape by 20, and 27 dB for the first and second fluidic circuits, respectively.

In recent years, an idea of integrating multi patches with different configurations has been investigated on cantilevered beams. Nestorović, Durrani, and Trajkov (2012) investigated four equals in length piezoelectric sensor actuator patches, two on each side, for active vibration control. On the other hand, the researchers Krott, Miura, Rahn, and Smith (2016); Miura, Krott, Smith, Rahn, and Romano (2015) studied passive vibration control by using two interconnected patches of F^2MC tubes with different configurations, their results agreed with present results. Then researchers focused on active or semi-active vibration control techniques for cantilever structures, to exemplify (Junda Chen et al., 2017) used Eddy Current Tuned Mass Dampers (ECTMDs) to control vibrations on cantilever beams. It composed of a small cantilever beam with magnet and cupper plat fixed on the free end of the primary cantilever beam, the authors adjusted the frequency of primary cantilever beam by variation the length of the small cantilever, which was also provide the stiffness of ECTMD. And the magnet was observed a lumped mass. In their results they proved that cantilever beams with ECTMD have more the equivalents damping ratios of 2.08~5.91 times that of the TMDs.

To the authors' best knowledge, there is no study in the literature which studied the performance of F^2MC tubes when composed of two respective fiber reinforced layers followed by one liner layer, filled with glycerin as working medium. The current paper is the first to do so. In this study three different models of F^2MC tubes were examined on the analyzed model in the literature (Bin Zhu, Rahn, & Bakis, 2015), with changing a composite layer material type, fluid type and some geometry parameters. Then a new analytical model for the cantilever beam was formulated by using multi-F^2MC tubes patches. The derived model equations were solved by using MATLAB software function solvers to obtain overall system transfer function as a ratio of tip unit displacement per unit of applied and presented by FRF plot. The tubes are modeled as three- layer tube. Investigations was done on the F^2MC tube's internal diameter whereas the other layers diameters were calculated as a function of the selected layer thickness ratios. Comparisons were performed between the models of one long patch of F^2MC tubes with a new model of two patches with a length of each of them as a half of the first model. Finally, variation of number of tubes inside each patch were studied. Model validations are captured

analytically by depending on previously done studies. The dynamic response of the structure with F^2MC tubes attached is drawn using FRF plot.

2. MATHEMATICAL MODELLING

This study deals with integrating two patches of F^2MC tubes on the uniform cantilever beam, each consists of a pair of three layered F^2MC tubes, the first two respective layers are composite laminate fiber reinforced layers followed by an outer liner layer, surrounding a working fluid (glycerin). The tubes are connected in parallel, flow inside them is controlled by orifice through an accumulator. The patches are fully separated, the fluid inside them are not mixed together. They act as two separate fluidic systems to suppress vibrations that occur by beam bending with an action of applied point load.

2.1 Beam Model

Figure 1 and Figure 2 show the patches of F^2MC tubes. They assumed stiff and fixed very well on the beam. So, when the applied load (F) acts on the beam, they remain fixed in their positions during bending of the beam. This bending due to extension of the F^2MC tubes in each system by an amount of (F_{t1}, and F_{t2}), and each results a formulation of a moments (M1) and (M2) in F^2MC tubes bonding position as;

$$M1=F_{t1}\times d \tag{1}$$

$$M2=F_{t2}\times d \tag{2}$$

where (d) is the distance between the neutral axis of the tubes and the center line of the beam.

Using Euler-Bernoulli beam theory the governing equations of transverse displacement $y_{(x,t)}$ is formulated as:

$$m\frac{d^2y}{dt^2}+B\frac{dy}{dt}+EI\frac{d^4y}{dx^4}=0 \text{ for } x\in(0,L). \tag{3}$$

where

$$m=\rho\times b\times h \tag{4}$$

taking the Laplace transform and solving for zero initial conditions

$$ms^2Y+BsY+EI\frac{d^4Y}{dx^4}=0 \tag{5}$$

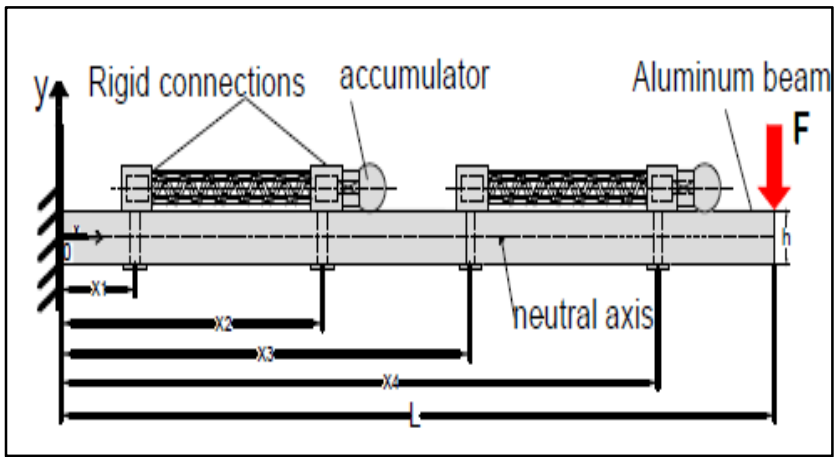

Figure 1: F^2MC Tubes Integrated on Cantilever Beam

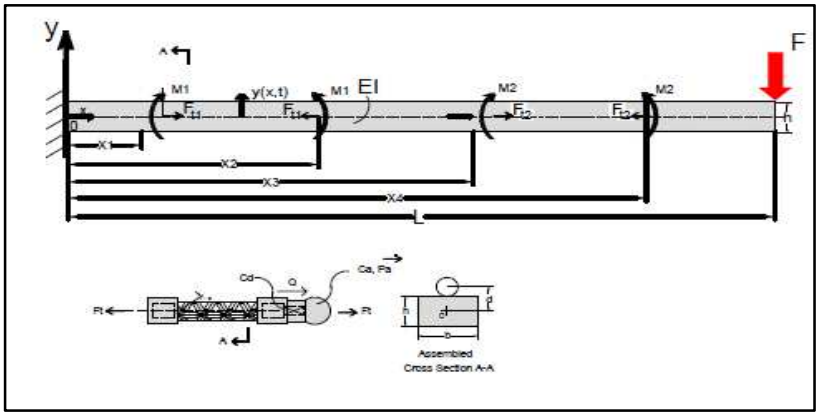

Figure 2: Free Body Diagram of Cantilever Beam with Integrated F²MC Tubes, Explaining Forces, Moments and Attaching Tubes Locations on it.

and rearranging

$$\frac{d^4Y}{dx^4}-\beta^4Y(x)=0 \tag{6}$$

where

$$\beta^4=\frac{s^2m+sB}{EI} \tag{7}$$

The generalized solution of the beam has five domains:

$$Y=\begin{cases} Y1(x,s)=A1\sin\beta x+A2\cos\beta x+A3\sinh\beta x+A4\cosh\beta x, \text{ for } x\epsilon(0,x_1) \\ Y2(x,s)=B1\sin\beta x+B2\cos\beta x+B3\sinh\beta x+B4\cosh\beta x, \text{ for } x\epsilon(x_1,x_2) \\ Y3(x,s)=C1\sin\beta x+C2\cos\beta x+C3\sinh\beta x+C4\cosh\beta x, \text{ for } x\epsilon(x_2,x_3) \\ Y4(x,s)=D1\sin\beta x+D2\cos\beta x+D3\sinh\beta x+D4\cosh\beta x, \text{ for } x\epsilon(x_3,x_4) \\ Y5(x,s)=E1\sin\beta x+E2\cos\beta x+E3\sinh\beta x+E4\cosh\beta x, \text{ for } x\epsilon(x_4,L) \end{cases} \tag{8}$$

The constants An, Bn, Cn Dn, and En for (n=1, 2, 3, 4) are found by using beam boundary conditions, (Gere, 2004):

In the left side of the beam (x=0) the beam is clamped, so

$$Y1(0,s)=0, \tag{9}$$

$$Y1'(0,s)=0. \tag{10}$$

Moment balance at $x = x_1$

$$EI(Y2''(x_1,s)-Y1''(x_1,s)=M1(s) \tag{11}$$

where $M(s)= \mathcal{L}M(t)$, by continuity

$$Y1(x_1,s)=Y2(x_1,s) \tag{12}$$

$$Y1'(x_1,s)=Y2'(x_1,s) \tag{13}$$

$$Y1'''(x_1,s)=Y2'''(x_1,s) \tag{14}$$

Moment balance at $x = x_2$ led to

$$EI(Y2''(x_2,s)-Y3''(x_2,s)=M1(s) \quad (15)$$

and the continuity due to

$$Y2(x_2,s)=Y3(x_2,s) \quad (16)$$

$$Y2'(x_2,s)=Y3'(x_2,s) \quad (17)$$

$$Y2'''(x_2,s)=Y3'''(x_2,s) \quad (18)$$

Moment balance at x=x3

$$EI(Y4''(x_3,s)-Y3''(x_3,s)=M2(s) \quad (19)$$

and the continuity due to

$$Y3(x_3,s)=Y4(x_3,s) \quad (20)$$

$$Y3'(x_3,s)=Y4'(x_3,s) \quad (21)$$

$$Y3'''(x_3,s)=Y4'''(x_3,s) \quad (22)$$

Moment balance at $x=x_4$

$$EI(Y4''(x_4,s)-Y5''(x_4,s)=M2(s) \quad (23)$$

and continuity gives

$$Y4(x_4,s)=Y5(x_4,s) \quad (24)$$

$$Y4'(x_4,s)=Y5'(x_4,s) \quad (25)$$

$$Y4'''(x_4,s)=Y5'''(x_4,s) \quad (26)$$

At free end, x=L

$$EIY5'''(L,s)=F(s) \quad (27)$$

$$EIY5''(L,s)=0 \quad (28)$$

2.2 Three Layered F^{2}MC Tube Model

Figure 1 shows that the patches are integrated on the beam, each consist of a pair of F^{2}MC tubes connected in parallel. The F^{2}MC tube is modelled as a structure that consists of three coaxial boundless length hollow cylinders perfectly bonded together: the inner and middle cylinders are FMC laminate, both are made from polyacrylonitrile-based carbon fiber. They are orthotropic, with reinforcing fibres oriented at $\pm\alpha$ to the axial direction of the tube; the outer liner cylinder is made from polyurethane (Figure 3-B). Each cylinder represents a layer, and the radii of layers from inside to outside are c_1, c_2, c_3 and c_4 respectively. The axial force exerted on the F^{2}MC tube balances the force on the individual tube layers,

$$T=T_1+T_2+T_3 \quad (29)$$

For two layered F^{2}MC tubes, the axial force can be found by summing only T_1 and T_2.

2.2.1 Inner and Middle Layers

Figure 2 highlights that the FMC inner layer is subjected to axial force (T_1), internal surface pressure (p_o) and external surface pressure (p_1). The axial force is:

$$T_1=2\pi \int_{c_1}^{c_2} \sigma_z^i c dc, \tag{30}$$

where σ_z^i represents the axial stress in the inner layer.

Furthermore, Lekhnitskii's elasticity solution for homogenous orthotropic cylinders was used to find the generalized stress distributions(Lekhnitskii, 1977), as:

$$\sigma_r^i=\frac{p_0 a^{k+1}-p_1}{1-a^{2k}}\mu^{k-1}+\frac{p_1 a^{k-1}-p_0}{1-a^{2k}}a^{k+1}\mu^{-k-1}+AhK_1, \tag{31}$$

$$\sigma_\theta^i=\frac{p_0 a^{k+1}-p_1}{1-a^{2k}}k\mu^{k-1}-\frac{p_1 a^{k-1}-p_0}{1-a^{2k}}ka^{k+1}\mu^{-k-1}+AhK_2, \tag{32}$$

$$\sigma_z^i=A-\frac{1}{b_{33}}\left(b_{13}\sigma_r^i+b_{23}\sigma_\theta^i\right), \tag{33}$$

where r, θ and z indicate radial, hoop and axial directions (Figure 3-B),

$$a=\frac{c_1}{c_2}, \tag{34}$$

$$\mu=\frac{c}{c_2}, \tag{35}$$

$$k=\sqrt{\frac{\beta_{11}}{\beta_{22}}}, \tag{36}$$

$$h=\frac{b_{23}-b_{13}}{\beta_{11}-\beta_{22}}, \tag{37}$$

$$\beta_{11}=b_{11}-\frac{b_{13}^2}{b_{33}}, \tag{38}$$

$$\beta_{22}=b_{22}-\frac{b_{23}^2}{b_{33}}, \tag{39}$$

$$K_1=1-\frac{1-a^{k+1}}{1-a^{2k}}\mu^{k-1}-\frac{1-a^{k-1}}{1-a^{2k}}a^{k+1}\mu^{-k-1}], \tag{40}$$

$$K_2=1-\frac{1-a^{k+1}}{1-a^{2k}}k\mu^{k-1}+\frac{1-a^{k-1}}{1-a^{2k}}ka^{k+1}\mu^{-k-1}], \tag{41}$$

The b_{ij} terms are three-dimensional effective compliance constants found from the homogenous properties of the inner layer in the cylindrical coordinate system (Bakaiyan, Hosseini, & Ameri 2009; Sun & Li, 1988). The transversely isotropic unidirectional reinforced $(+\alpha)$ and $(-\alpha)$ sub-layers are assumed for calculating the homogenous properties of $\pm\alpha$ composite layers. Therefore, the layers have five independent elastic constants: longitudinal and transverse modulus of elasticity E_{11}, E_{22}, Poisson's ratio ν_{12} and ν_{23} and longitudinal shear modulus of elasticity G_{12}.

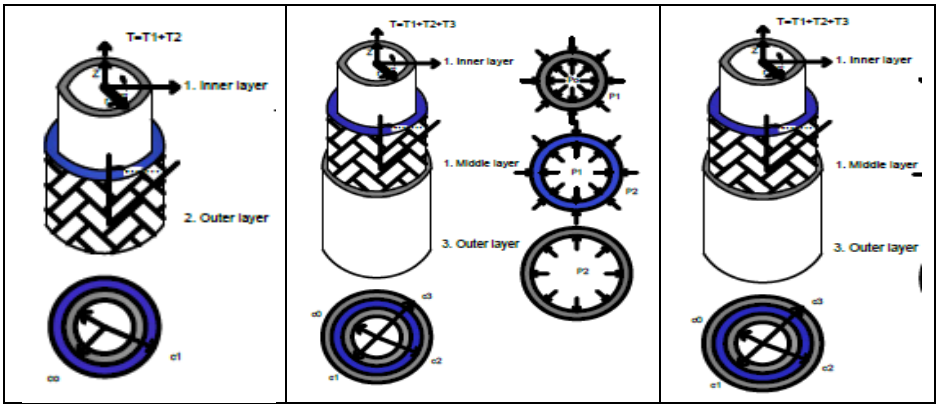

(A) Two Layer Model **(B) Three Layer (Mathematically Modelled)** **(C) Three Layer (base line)**

Figure 3: The Studied Models of the Tube

Solving the equations (30-33) lead to finding the parameter (A) as a function of (T_1, p_0 and p_1). The strain distributions for the inner composite layer are:

$$\varepsilon_r^i=b_{11}\sigma_r^i+b_{12}\sigma_\theta^i+b_{13}\sigma_z^i, \tag{42}$$

$$\varepsilon_\theta^i=b_{12}\sigma_r^i+b_{22}\sigma_\theta^i+b_{23}\sigma_z^i, \tag{43}$$

$$\varepsilon_z^i=b_{13}\sigma_r^i+b_{23}\sigma_\theta^i+b_{33}\sigma_z^i, \tag{44}$$

Similarly, the axial force (T_2), stresses $(\sigma_r^m, \sigma_\theta^m, \sigma_z^m)$ and strains $(\varepsilon_r^m, \varepsilon_\theta^m, \varepsilon_z^m)$ for the middle reinforced layer are found by replacing$(T_1, p_0, p_1, c_1$ and $c_2)$ with $(T_2, p_1, p_2, c_2$ and $c_3)$ respectively in Eqs. (30-44).

2.2.2 Outer Layer

This layer is modelled as an infinitely long isotropic hollow cylinder with an axial force (T_3), inside and outside surface pressures (p_2) and $(p_3 = 0)$(Figure 3-B)Therefore, relying on (Boresi, Schmidt, & Sidebottom, 1993), the stress distributions are:

$$\sigma_r^o=\frac{p_2c_3^2-p_3c_4^2}{c_4^2-c_3^2}-\frac{c_3^2c_4^2(p_2-p_3)}{c^2(c_4^2-c_3^2)}, \tag{45}$$

$$\sigma_\theta^o=\frac{p_2c_3^2-p_3c_4^2}{c_4^2-c_3^2}+\frac{c_3^2c_4^2(p_2-p_3)}{c^2(c_4^2-c_3^2)}, \tag{46}$$

$$\sigma_z^o=\frac{T_3}{\pi(c_4^2-c_3^2)}, \tag{47}$$

The strains in each direction can be obtained by using Hooke's law

$$\varepsilon_r^o=\frac{1}{E_o}[\sigma_r^o-\nu_o(\sigma_\theta^o+\sigma_z^o)], \tag{48}$$

$$\varepsilon_\theta^o=\frac{1}{E_o}[\sigma_\theta^o-\nu_o(\sigma_r^o+\sigma_z^o)], \tag{49}$$

$$\varepsilon_z^o=\frac{1}{E_o}[\sigma_z^o-\nu_o(\sigma_\theta^o+\sigma_r^o)], \tag{50}$$

where $(E_oE_oE_oE_oE_oE_oE_oE_o)$ and $(\nu_o\nu_o\nu_o\nu_o\nu_o\nu_o\nu_o\nu_o)$ are Young's modulus of elasticity and Poisson's ratio for

polyurethane respectively.

2.3 Equilibrium Equations

In this model, each F^{2}MC patch follows a plain strain solution, as the beam extends uniformly in an axial direction, therefore:

$$\varepsilon_z^i=\varepsilon_z^m, \tag{51}$$

$$\varepsilon_z^m=\varepsilon_z^o. \tag{52}$$

At the interface between any two layers the hoop strains are identical,

$$\varepsilon_\theta{}^i\big|_{c=c_2} = \varepsilon_\theta{}^m\big|_{c=c_2} \tag{53}$$

$$\varepsilon_\theta{}^m\big|_{c=c_3} = \varepsilon_\theta{}^o\big|_{c=c_3} \tag{54}$$

The axial force on each F^{2}MC patch balances the loads on the end of the F^{2}MC tube,

Table 1: Model Parameters and Material Properties of F^{2}MC Tubes

Parameter	Symbol	Quantity
Fiber Reinforced Layer		
longitudinal modulus of elasticity (GPa)	E_{11}	40
transverse modulus of elasticity (MPa)	E_{22}	1.8
poisons ratio	v12	0.33
poisons ratio	v23	0.39
modulus of rigidity (MPa)	G_{12}	1.4
fiber angle (°)	α	±27
Liner Layer		
modulus of elasticity (MPa)	E_o	11
poisons ratio	v_o	0.498
F^{2}MC Tube Geometry and its Attaching Points		
inner layer internal radius(mm)	c1	0.54
middle layer internal radius (mm)	c2	0.9
outer layer internal radius(mm)	c3	1.28
outer radius (mm)	c4	1.406
first integration point of the patch(mm)	x_1	0
Second integration point of the patch(mm)	x_2	150
F^{2}MC tube length (mm)	L_{FMC}	150
Aluminum Beam Properties		
modulus of elasticity (GPa)	E	70
damping constant (N. s/m)	C	0.2
Density (kg/m^3)	ρ	2700
cross sectional height (mm)	h	1.6
Cross sectional width (mm)	b	26
length of the beam	L	310
Fluid Properties		
Type of fluid	glycerine	
Density (kg/m^3)	ρ	1260
bulk modulus (GPa)	B	4.35
accumulator capacitance (m3/Pa)	Ca	1.5×10^{-9}
Flow coefficient (m3/s Pa)	C_d	2×10^{-13}

$$T_1=\frac{Ft_1}{N}+ p_o\pi c_1^2 \tag{55}$$

$$T_2=\frac{Ft_2}{N}+p_o\pi c_1^2 \tag{56}$$

where (p_o) is fluid pressure inside the tubes and (N) is the number of tubes. By given geometry and material properties (Table 1), the axial and hoop strains of the inner layer can be calculated by solving eq.(51–56) as functions of (T and p_0) as

$$\varepsilon_{\theta 1}|_{r=c_1}=\emptyset_1 T_1+\emptyset_2 p_0 \tag{57}$$

$$\varepsilon_{\theta 2}|_{r=c_1}=\emptyset_1 T_2+\emptyset_2 p_0 \tag{58}$$

and

$$\varepsilon_{z1}=\emptyset_3 T_1+\emptyset_4 p_0 \tag{59}$$

$$\varepsilon_{z2}=\emptyset_3 T_2+\emptyset_4 p_0 \tag{60}$$

where $\varepsilon_{\theta 1}, \varepsilon_{\theta 2,} \varepsilon_{z1}$, and ε_{z2} are strains in hub and axial directions for first and second patches respectively, and $\emptyset_1, \emptyset_2, \emptyset_3$ and $\emptyset_4$ are constants representing the geometry and material properties of the F^{2}MC tubes for all patches.

2.4 Fluid Behavior

The study includes multi-F^{2}MC patch model in a closed valve scenario. It is assumed that the tubes are filled with fluid, are tight with no differential pressure with the bulk modulus (B) and volume of (V_i). When the force (F) is applied, the volume of the F^{2}MC tubes changes by the amount of (ΔV_f) with the formation of (F_{t1}, and F_{t2}). Depending on the volume change, the fluid differential pressure changes from zero to (p_0). For first patch, this can be expressed as:

$$\left(\frac{\Delta V_f}{V_{i1}}\right)B=-p_0, \tag{61}$$

but the volume change of F^{2}MC tube is defined as:

$$\Delta V_1=V_1-V_{i1}, \tag{62}$$

where

$$V_1=\pi\left[\left(1+\varepsilon_{\theta 1}|_{r=c_1}\right)c_1\right]^2(x2-x1)(1+\varepsilon_z), \tag{63}$$

$$V_{i1}=\pi c_1^2(x2-x1). \tag{64}$$

For second patch, the procedure is the same only the bonding positions are changed:

$$\Delta V_2=V_2-V_{i2}, \tag{65}$$

$$V_2=\pi\left[\left(1+\varepsilon_{\theta 2}|_{r=c_1}\right)c_1\right]^2(x4-x3)(1+\varepsilon_z), \tag{66}$$

$$V_{i2}=\pi c_1^2(x4-x3). \tag{67}$$

then the volume ratio for each F^{2}MCpatch can be written as:

$$\frac{\Delta V_1}{V_{i1}}=\frac{V_{i1}-V_1}{V_{i1}}\cong\varepsilon_{z1}+2\varepsilon_{\theta 1}|_{r=c_1}, \tag{68}$$

$$\frac{\Delta V_2}{V_{i2}}=\frac{V_{i2}-V_2}{V_{i2}}\cong \varepsilon_{z2}+2\varepsilon_{\theta 2}|_{r=c_1} \quad (69)$$

The fluid volume that is pumped out of the first and second patches, which are composed of (N) tubes, was assumed as the fluid volume flow rate and expressed as

$$Q_{v1}= -N\left(\Delta V_1-\Delta V_f\right). \quad (70)$$

$$Q_{v2}= -N(\Delta V_2-\Delta V_f). \quad (71)$$

by substituting each of ΔV_f and ΔV_1 and ΔV_2 from equations (61), (62) and (65)respectively, yields

$$\dot{Q}_{v1}=NF_Q\dot{T}+NG_Q\dot{p_0} = \dot{Q}_{v2} \quad (72)$$

where

$$G_Q=-(2\emptyset_1+\emptyset_3)V_{in} \quad (73)$$

$$F_Q=-(\emptyset_2+2\emptyset_4+\frac{1}{B})V_{in} \quad (74)$$

where $V_{in} = V_{i1}$ or V_{i2}, depending on the selected patch.

As the fluids inside both patches are the same type with the same configuration, the fluid volume flow rate balances the change in fluid pressure inside the orifice and accumulator by,

$$Q_v=C_d(p_0-p_A) \quad (75)$$

and

$$Q_v=C_a\dot{p_A} \quad (76)$$

where (p_A) is the internal pressure of the accumulator, (C_d) the flow coefficient and (C_a) is the accumulator capacity.

2.5 Over All System's Transfer Function

The transfer function of patches can be determined by the ratio of the axial strain to the axial force by solving each of equations (55), (59), (72), (75)and (76), also (56), (60), (72), (75) and (76) in the Laplace domain with zero initial conditions for first and second patches respectively as follows:

$$\varepsilon_{z1}(s)= G_p(s)F_{t1}(s), \text{ and}\varepsilon_{z2}(s)= G_p(s)F_{t2}(s) \quad (77)$$

where

$$G_p(s)=\frac{(c_as+c_d)(\emptyset_3F_Q-\emptyset_4G_Q)-\theta_3c_ac_d/N}{N(c_as+c_d)(F_Q+\pi c_1^2G_Q)-c_ac_d} \quad (78)$$

As required by Lekhnitskii's theory of elasticity (Lekhnitskii, 1977), the patches stretch uniformly in an axial direction, and the total F^2MC tube patch elongation can be calculated as,

$$\Delta L_1(s)=L_{FMC1}\varepsilon_{z1}(s)= -d(\frac{dY_2(s)}{dx2}-\frac{dY_2(s)}{dx1}), \quad (79)$$

$$\Delta L_2(s)=L_{FMC2}\varepsilon_{z2}(s)= -d(\frac{dY_4(s)}{dx4}-\frac{dY_4(s)}{dx3}), \quad (80)$$

where $L_{FMC1}=(x_2-x_1)$, and $L_{FMC2}=(x_4-x_3)$

substituting (F_{t1}) and (d) in equations (77) and (79) into equation (1) then solving for moment (M1), and substituting (F_{t1}) and (d) in equations (77) and (80) into equation (2) then solving for moment (M2), yield the following equations:

$$M1(s)=\frac{1}{U1(s)}\left[\frac{dY_2(s)}{dx2}-\frac{dY_2(s)}{dx1}\right], M2(s)=\frac{1}{U2(s)}\left[\frac{dY_4(s)}{dx4}-\frac{dY_4(s)}{dx3}\right], \quad (81)$$

where

$$U1(s)=\frac{L_{FMC1}}{d^2}G_p(s),\ U2(s)=\frac{L_{FMC2}}{d^2}G_p(s) \quad (82)$$

Now, substituting equation (81) into the constants equations (9) – (28) the following expression can be obtained:

$$J\ w=b\ F(s), \quad (83)$$

where

$$J=\begin{bmatrix}
0 & 1 & 0 & 1 & 0 & 0 & 0 & 0 & 0 & 0 & 0 & 0 & 0 & 0 & 0 & 0 & 0 & 0 & 0 & 0\\
1 & 0 & 1 & 0 & 0 & 0 & 0 & 0 & 0 & 0 & 0 & 0 & 0 & 0 & 0 & 0 & 0 & 0 & 0 & 0\\
J_{31} & J_{32} & J_{33} & J_{34} & J_{35} & J_{36} & J_{37} & J_{38} & 0 & 0 & 0 & 0 & 0 & 0 & 0 & 0 & 0 & 0 & 0 & 0\\
J_{41} & J_{42} & J_{43} & J_{44} & J_{45} & J_{46} & J_{47} & J_{48} & 0 & 0 & 0 & 0 & 0 & 0 & 0 & 0 & 0 & 0 & 0 & 0\\
J_{51} & J_{52} & J_{53} & J_{54} & J_{55} & J_{56} & J_{57} & J_{58} & 0 & 0 & 0 & 0 & 0 & 0 & 0 & 0 & 0 & 0 & 0 & 0\\
J_{61} & J_{62} & J_{63} & J_{64} & J_{65} & J_{66} & J_{67} & J_{68} & 0 & 0 & 0 & 0 & 0 & 0 & 0 & 0 & 0 & 0 & 0 & 0\\
0 & 0 & 0 & 0 & J_{75} & J_{76} & J_{77} & J_{78} & J_{79} & J_{710} & J_{711} & J_{712} & 0 & 0 & 0 & 0 & 0 & 0 & 0 & 0\\
0 & 0 & 0 & 0 & J_{85} & J_{86} & J_{87} & J_{88} & J_{89} & J_{810} & J_{811} & J_{812} & 0 & 0 & 0 & 0 & 0 & 0 & 0 & 0\\
0 & 0 & 0 & 0 & J_{95} & J_{96} & J_{97} & J_{98} & J_{99} & J_{910} & J_{911} & J_{912} & 0 & 0 & 0 & 0 & 0 & 0 & 0 & 0\\
0 & 0 & 0 & 0 & J_{105} & J_{106} & J_{107} & J_{108} & J_{109} & J_{1010} & J_{1011} & J_{1012} & 0 & 0 & 0 & 0 & 0 & 0 & 0 & 0\\
0 & 0 & 0 & 0 & 0 & 0 & 0 & 0 & J_{119} & J_{1110} & J_{1111} & J_{1112} & J_{1113} & J_{1114} & J_{1115} & J_{1116} & 0 & 0 & 0 & 0\\
0 & 0 & 0 & 0 & 0 & 0 & 0 & 0 & J_{129} & J_{1210} & J_{1211} & J_{1212} & J_{1213} & J_{1214} & J_{1215} & J_{1216} & 0 & 0 & 0 & 0\\
0 & 0 & 0 & 0 & 0 & 0 & 0 & 0 & J_{139} & J_{1310} & J_{1311} & J_{1312} & J_{1313} & J_{1314} & J_{1315} & J_{1316} & 0 & 0 & 0 & 0\\
0 & 0 & 0 & 0 & 0 & 0 & 0 & 0 & J_{149} & J_{1410} & J_{1411} & J_{1412} & J_{1413} & J_{1414} & J_{1415} & J_{1416} & 0 & 0 & 0 & 0\\
0 & 0 & 0 & 0 & 0 & 0 & 0 & 0 & 0 & 0 & 0 & 0 & J_{1513} & J_{1514} & J_{1515} & J_{1516} & J_{1517} & J_{1518} & J_{1519} & J_{1520}\\
0 & 0 & 0 & 0 & 0 & 0 & 0 & 0 & 0 & 0 & 0 & 0 & J_{1613} & J_{1614} & J_{1615} & J_{1616} & J_{1617} & J_{1618} & J_{1619} & J_{1620}\\
0 & 0 & 0 & 0 & 0 & 0 & 0 & 0 & 0 & 0 & 0 & 0 & J_{1713} & J_{1714} & J_{1715} & J_{1716} & J_{1717} & J_{1718} & J_{1719} & J_{1720}\\
0 & 0 & 0 & 0 & 0 & 0 & 0 & 0 & 0 & 0 & 0 & 0 & J_{1813} & J_{1814} & J_{1815} & J_{1816} & J_{1817} & J_{1818} & J_{1819} & J_{1820}\\
0 & 0 & 0 & 0 & 0 & 0 & 0 & 0 & 0 & 0 & 0 & 0 & 0 & 0 & 0 & 0 & J_{1917} & J_{1918} & J_{1919} & J_{1920}\\
0 & 0 & 0 & 0 & 0 & 0 & 0 & 0 & 0 & 0 & 0 & 0 & 0 & 0 & 0 & 0 & J_{2017} & J_{2018} & J_{2019} & J_{2020}
\end{bmatrix},\ w=\begin{bmatrix}A1\\A2\\A3\\A4\\B1\\B2\\B3\\B4\\C1\\C2\\C3\\C4\\D1\\D2\\D3\\D4\\E1\\E2\\E3\\E4\end{bmatrix},\ b=\begin{bmatrix}0\\0\\0\\0\\0\\0\\0\\0\\0\\0\\0\\0\\0\\0\\0\\0\\0\\0\\0\\0\\\frac{1}{EIβ^3}\\0\end{bmatrix} \quad (84)$$

and

$J_{31}=U1EIβSβx_1$
$J_{32}=U1EIβCβx_1$
$J_{33}=-U1EIβShβx_1$
$J_{34}=-U1EIβChβx_1$
$J_{35}=-U1EIβSβx_1 - Cβx_2+Cβx_1$
$J_{36}=-U1EIβCβx_1+Sβx_2 - Sβx_1$
$J_{37}=U1EIβShβx_1 - Chβx_2+Chβx_1$
$J_{38}=U1EIβChβx_1 - Shβx_2+Shβx_1$
$J_{75}=-U1EIβSβx_2 - Cβx_2+Cβx_1$
$J_{76}=-U1EIβCβx_2+Sβx_2 - Sβx_1$
$J_{77}=U1EIβShβx_2 - Chβx_2+Chβx_1$
$J_{78}=U1EIβChβx_2 - Shβx_2+Shβx_1$
$J_{79}=U1EIβSβx_2$
$J_{710}=U1EIβCβx_2$
$J_{711}=-U1EIβShβx_2$
$J_{712}=-U1EIβChβx_2$
$J_{119} = U2EIβSβx_3$
$J_{1110}=U2EIβCβx_3$
$J_{1111}=-U2EIβShβx_3$
$J_{1112}=-U2EIβChβx_3$
$J_{1113}=-U2EIβSβx_3-Cβx_4+Cβx_3$
$J_{1114}=-U2EIβCβx_3+Sβx_4-Sβx_3$

$J_{41}=Sβx_1$
$J_{42}=Cβx_1$
$J_{43}=Shβx_1$
$J_{44}=Chβx_1$
$J_{45}= -Sβx_1$
$J_{46}=-Cβx_1$
$J_{47}= -Shβx_1$
$J_{48}= -Chβx_1$
$J_{85}=Sβx_2$
$J_{86}=Cβx_2$
$J_{87}=Shβx_2$
$J_{88}=Chβx_2$
$J_{89}=-Sβx_2$
$J_{810}=-Cβx_2$
$J_{811}=-Shβx_2$
$J_{812} =-Chβx_2$
$J_{129}=Sβx_3,$
$J_{1210}=Cβx_3$
$J_{1210}=Shβx_3$
$J_{1212}=Chβx_3$
$J_{1213}=-Sβx_3$
$J_{1214}=-Cβx_3$

$J_{51}=Cβx_1$
$J_{52}=-Sβx_1$
$J_{53}=Chβx_1$
$J_{54}=Shβx_1$
$J_{55}=-Cβx_1$
$J_{56}=Sβx_1$
$J_{57}=-Chβx_1$
$J_{58} =-Shβx_1$
$J_{95}=Cβx_2$
$J_{96}=-Sβx_2$
$J_{97}=Chβx_2$
$J_{98}=Shβx_2$
$J_{99}=-Cβx_2$
$J_{910}=Sβx_2$
$J_{911}=-Chβx_2$
$J_{912}=-Shβx_2$
$J_{139}=Cβx_3$
$J_{1310}=-Sβx_3$
$J_{1311}=Chβx_3$
$J_{1312}=Shβx_3$
$J_{1313}= -Cβx_3$
$J_{1314}=Sβx_3$

$J_{61}=-Cβx_1$
$J_{62}=Sβx_1$
$J_{63}=Chβx_1$
$J_{64}=Shβx_1$
$J_{65}=Cβx_1$
$J_{66}=-Sβx_1$
$J_{67}=-Chβx_1$
$J_{68}=-Shβx_1$
$J_{105}=-Cβx_2$
$J_{106}=Sβx_2$
$J_{107}=Chβx_2$
$J_{108}=Shβx_2$
$J_{109}=Cβx_2$
$J_{1010}=-Sβx_2$
$J_{1011}= -Chβx_2$
$J_{1012}= -Shβx_2$
$J_{149}=-Cβx_3$
$J_{1410}=Sβx_3$
$J_{1411}=Chβx_3$
$J_{1412}=Shβx_3$
$J_{1413}=Cβx_3,$
$J_{1414}=-Sβx_3$

J_{1115}=U2EIβShβx_3-Chβx_4+Chβx_3
J_{1116} =U2EIβChβx_3-Shβx_4+Shβx_3
J_{1513}=-U2EIβSβx_4 − Cβx_4 + Cβx_3
J_{1514}=-U2EIβCβx_4 + Sβx_4 − Sβx_3
J_{1515}=U2EIβShβx_4 − Chβx_4 + Chβx_3
J_{1516}=U2EIβChβx_4 − Shβx_4 + Shβx_3
J_{1517}=U2EIβSβx_4
J_{1518}=U2EIβCβx_4
J_{1519}=-U2EIβShβx_4
J_{1520}=-U2EIβChβx_4
J_{1917}=-EICβL
J_{1918}=EISβL
J_{1919}=EIChβL
J_{1920}=EIShβL

J_{1215}=-Shβx_3
J_{1216}=-Chβx_3
J_{1613}=Sβx_4
J_{1614}=Cβx_4
J_{1615}=Shβx_4
J_{1616}=Chβx_4
J_{1617}=-Sβx_4
J_{1618}=-Cβx_4
J_{1619}=-Shβx_4
J_{1620}=-Chβx_4
J_{2017}=-EISβL
J_{2018}=-EICβL
J_{2019}=EIShβL
J_{2020}=EIChβL.

J_{1315}= -Chβx_3
J_{1316}= -Shβx_3
J_{1713}=Cβx_4
J_{1714}=-Sβx_4
J_{1715}=Chβx_4
J_{1716}=Shβx_4
J_{1717}=-Cβx_4
J_{1718}=Sβx_4
J_{1719}= -Chβx_4
J_{1720}= -Shβx_4

J_{1415}=-Chβx_3
J_{1416} =-Shβx_3
J_{1813}=-Cβx_4
J_{1814}=Sβx_4
J_{1815}=Chβx_4
J_{1816}=Shβx_4
J_{1817}= Cβx_4
J_{1818}=-Sβx_4
J_{1819}= -Chβx_4
J_{1820}= -Shβx_4

where S, C, Sh, Ch, U1 and U2 are sin, cos, sinh, cosh, U1(s), and U2(s) respectively.

The total deflection at the free end of the beam is

$$Y(L,s)= E1\sin\beta L+E2\cos\beta L+E3\sinh\beta L+E4\cosh\beta L \quad (85)$$

and the overall transfer function of the F^2MC structure is

$$\frac{Y(L,s)}{F(s)}=a_w J^{-1} b=H(s) \quad (86)$$

with a_w=[0 0 0 0 0 0 0 0 0 0 0 0 0 0 0 0 sinβL cosβL sinhβL coshβL], and the FRF is represented by |H(jω)|.

3. MODEL VALIDATION

As producing F^2MC tubes samples are difficult. It requires sophisticated devices because of their size and layer thickness, the derived model validated theoretically by performing some illustrative examples and the results were compared with the existing data available in the literature to demonstrate the accuracy of the present model. As an example, comparisons are made between the FRF plot obtained from the previous studies and those obtained by(Bin Zhu et al., 2015) for F^2MC tubes integrated on the cantilever beam (Figure 4). It could be seen, the present results are in well agreement with similar ones available in previous studies in the reference, which had been agreed with their experimental validations. This agreement improved the proposal of a new model, strong enough to be used for future studies.

4. PARAMETRIC INVESTIGATIONS

This study involves improvements on the F^2MC tubes' performances when coupled to a fluid port and an air chamber as vibration absorber by the following examinations:

4.1 Changing the F^2MC Tube's Model

The present study examined the F^2MC tubes' performance for damping on validated model. Here only one patch integrated on the beam. The examination taken place by developing two different models of multi-layer F^2MC tubes: First composed of two layers (inner liner and outer composite laminate) and second consist of three layers (two respective fiber reinforced layers from inside to outside, followed by a liner layer), the details are shown in Figure 3. Their FRF response were compared with a base line model which also composed of three layers with only middle layer composite laminate (Figure

3-C). For all models, the materials are the same and detailed in Table 1. The F^{2}MC tube's material for fiber reinforced layers was selected as polyacrylonitrile based carbon fiber which has lower modulus of elasticity as compared to the material used in previous study. Whereas, the liner layer material is polyurethane. There are changes between the number and material type of layers. In the second model the inner layer thickness was approximately the sum of both inner and middle layer thicknesses of the tube in base line model. Because they made from the same material and perfectly bonded together, they can be assumed as thick two-layer tube.

Figure 5 shows the resulted FRF plot for all three models. The solid line is base line model. The thickness of layers of this model is different with the other two models. In the first model, inner liner layer is better for prevention of fluid's leakage than composite liner layer. The change in material and geometry of the tubes play a significant role on the F2MC tubes modulus ratio which is the ratio of the applied stress to the total amount of strain in the longitudinal direction (Y. Chen, Sun, Liu, & Leng, 2012; Ying Shan et al., 2009). Thin walled tubes with small fiber angles have large modulus ratios, and axial strain εz, as in base line model Figure 3-C. whereas, in the new three-layer model the walls are thicker. the thick wall provides radial compliance that assists the contraction/extraction performance, and increases the active volume fraction relative to the matrix material and thereby increases actuation(Bin Zhu, 2014) which directly achieves more damping. If the wall becomes too thick, the performance of the F^{2}MC tube begins to decrease. Because reduces the flexibility of the tubes. in the other hand within increasing the total thickness of tubes, modulus ratio is decreased thus damping is improved (Y. Chen et al., 2012). The dashed lines in FRF plot are representing two-layer model. It showed a 2.77dB reduction in amplitude of the first mode shape in comparison with the baseline model. The second model is illustrated by dash-dotted in the same figure, where it gained higher reduction in first mode shape. The first resonated amplitude was reduced by 12.12 dB in comparison with the base line model, with constant resonance frequency. The occurrence of this reduction can be referred to the material properties and thickness of inner layer, in addition to the high viscosity fluid that has been used inside the tubes. It increased internal friction with F^{2}MC tube walls which directly increases fluid drag forces (S. S. Chen, Wambsganss, M. W., Jendrzejczyk, J. A., 1976).

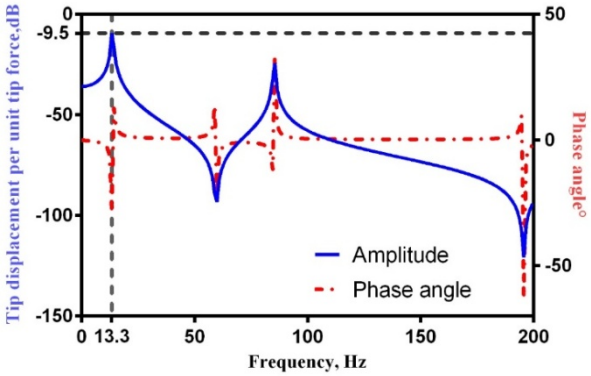

Figure 4: Frequency Response Plot for (Bin Zhu et al., 2015) Model for Comparison Purpose.

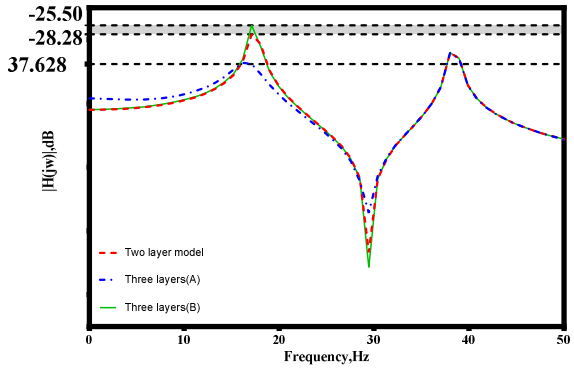

Figure 5: FRF Plot of Overall System with Different Models of F^{2}MC Tubes: Two-layer Model with Inner Liner with Outer Fiber Reinforced Layer (dashed), two Composite Laminate Layers Followed by one liner Layer (dash-doted); Base Line Model (solid line).

However, this force losses at support points, but this event is small if compared with fluid viscosity effects. Supports the direct relation between fluid viscosity and damping coefficient. This relation was also reported by Miller

when it was compared some other liquids with water under the same conditions (Miller, 1965). Although, this model was stiffer inside however the whole system behaved as a flexible system. This could be due to that the increasing stiffness to a certain limit caused by reducing volume change and facilitating the generation of high internal pressures which increases damping. This comparison gives the opportunity to the modeled three-layer F^2MC tubes for damping more than two-layer model of F^2MC tubes. These results are in a good agreement with the findings of previous researchers (Krott et al., 2015).

4.2 Multi Patch Model

The study examined integrating two patches on the beam. Each with properties detailed as the second model in previous section. One long patch with pair of F^2MC tubes, is replaced with two short identical patches, consisting of a single tube and having half length of the long patch. Here larger tubes are used (Table 2). The two models have similar geometry and material properties. During bending the transverse vibrations that obtained were extended the patches not equally, this caused the formulation of moments M1and M2 at the bonding points of each patch instead of a moment from one patch.

Table 2: Base Line Parameters of Multi Patch Model of F^2MC Tubes

F^2MC Tube Radius		
inner layer internal radius(mm)	c1	1
middle layer internal radius(mm)	c2	1.7 c1
outer layer internal radius(mm)	c3	1.8 c1
outer radius (mm)	c4	2.105 c1
First Patch Location Points		
Distance from the fixed end to its first location point (mm)	x_1	0
Distance from the fixed end to its second location point (mm)	x2	75
total length of first patch(mm)	x_2-x_1	75
Second Patch Location Points		
Distance from the fixed end to its first location point (mm)	x_3	110
Distance from the fixed end to its second location point (mm)	x_4	185
total length of second patch (mm)	x4-x3	75

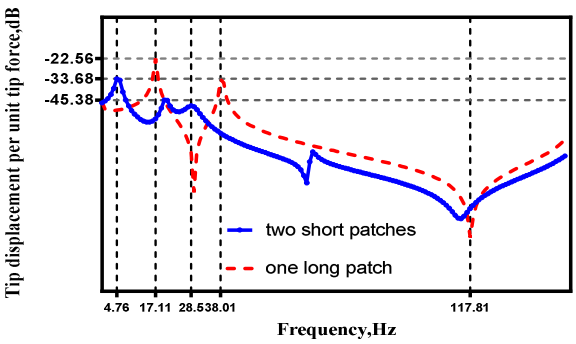

Figure 6: Comparison Between Two Configurations: (solid) for Two 75mm long Similar Patches, 35cm apart, Bonded on the Cantilever Beam. And (dashed) for One Long Patch 150mm. Each Patch Contains a pair of F^2MC tubes. The Working Fluid is Glycerin.

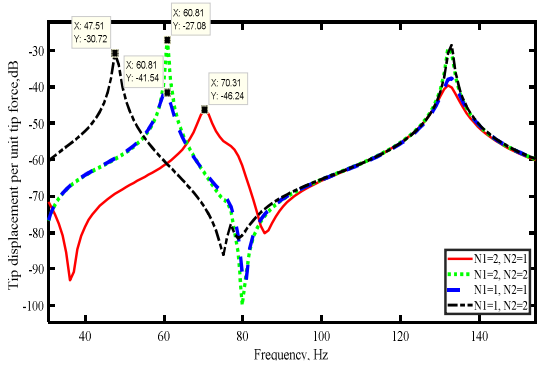

Figure 7: Amplitude of System Response by using Two Patches of F^2MC Tubes Bonded in series with a Distance of 35mm Between them, for Different Number of the Tubes in Each Patch: N1=2, N2=1 (solid); N1=N2=2 (dotted); N1=N2=1(dashed); N1=1, N2=2 (dash-dotted).

Thus, the resulted moments along with a beam adds more damping than one concentrated moment. With the comparison in results, reductions in amplitudes of first and second mode shapes by 11.12, 11.7 dB with shifts in first and

second resonance frequencies by 12.41 and 18 Hz respectively, were recorded. In addition to a reduction in overall gain between 40Hz~110Hz (Figure 6). Among the two examined cases, in spite of having the same patch length and size.

The reason of innovations could be related to the technique of integrating the patches on the beam. In the case of integrating two patches, the beam deflection caused an increase in fluid flow into the patches. However, the closer patch to the free end of the beam will be followed by generation of more fluid flow than the other patch. As the patches are separated, there will be a difference in moments M1and M2 Eq. (1–2), in a way that M1 is greater than M2, because it is more far away from the point of action of applied force than M2. As a result, more damping was achieved in addition to overall gain reduction, when it was compared with integrating one long patch on the same beam.

4.3 Configuration of Variation of the Number of Tubes

As it can be notified from the recent studies all researchers used a pair of F^2MC tubes for vibration control configuration. In better words, there is no study which deals with changing the number of tubes inside F^2MC patches. This study focused on comparison between using one tube or two tubes in each patch design. In contrast, changing the number of tubes in the patches dramatically change both first resonance amplitude as well as frequency (Figure 7). In the case of having two patches, because the patches are fully separated, they are not interconnected. The fluid inside each patch is enclosed, it's transportation between the patches is impossible. There is only fluid flow between the tubes connected in parallel in each patch. As shown in Figure 7, when the number of tubes inside each patch are equal, the same resonance frequency of first mode shape was obtained with lower amplitude of vibration (14 dB) in case of having single tubes than a pair of tube in each patch. Because in the case of having two tubes in a patch, with constant volume of fluid, the fluid distribution between the two tubes, directly reduces the amount of fluid flow entering each tube, generating lower pressures inside the tubes which minimizes the moments M1 and M2 that obtained in bonding points; following a resulted lower beam damping. While in the case of different number of tubes in each patch, the usage of pair of F^2MC tubes inside the first patch improves more damping than the second patch. There is a shift in resonance frequency by 22.8Hz with lower amplitude of resonance by 15.48dB, that is because of having larger bending in the points of integrating second patch that first patch, as it is closer to the free end of the beam.

5. CONCLUSIONS

This study represents a valuable approach for damping cantilever beam vibrations in a simple way through integration of F^2MC tubes on it. The new model of multi-layer F^2MC tubes was investigated, composed of two respective fiber reinforced layers, surrounding one liner layer, enclosing glycerin as working fluid inside them. New mathematical model of integrating two separate patches of F^2MC tubes were formulated by depending of the basics of integrating a single patch. Beam damping obtained by entering fluid into the F^2MC tubes, and pressure generation inside each of them, through formulation of transverse vibrations obtained by beam bending. There is a relationship between the tubes thickness of layers and their performance for damping. Thick F^2MC tubes are more effective for damping than thinner once. The study improved beam damping with an overall reduction in first resonance amplitudessignificantly. Replacing one long patch by two separate short patches because powerful changes in overall response in the systems FRF plot. The study achieved reductions in amplitude and frequency of resonance in first mode shapes by 20.7dB and 53Hz, respectively.

REFERENCES

1. *Bakaiyan, H., Hosseini, H., & Ameri, E. (2009). Analysis of multi-layered filament-wound composite pipes under combined*

internal pressure and thermomechanical loading with thermal variations. Composite Structures, 88(4), 532–541 doi:10.1016/j.compstruct.2008.05.017

2. *Bhagat, V. K., Prasad, A. K., & Srivastava, A. K. L. Influence Of Moisture Absorption And Their Effect On The Physho-Mechanical Properties Of Coir-Luffa Fibre Reinforced Polymer Matrix Composites.*
3. *Boresi, A. P., Schmidt, R. J., & Sidebottom, O. M. (1993). Advanced Mechanics of materials (5th ed.). USA: John Willey & Sons Inc.*
4. *Chen, S. S., Wambsganss, M. W., Jendrzejczyk, J. A.,. (1976). Added mass and damping of a vibrating rod in confined viscous fluids. Journal of Applied Mechanics, 43(2), 325–329.*
5. *Chen, Y., Sun, J., Liu, Y., & Leng, J. (2012). Experiment and analysis of fluidic flexible matrix composite (F2MC) tube. Journal of Intelligent Material Systems and Structures. doi:10.1177/1045389X11420591*
6. *Gere, J. M. (2004). Mechanics of Materials (6th ed.): Thomson Brooks/Cole.*
7. *Junda Chen, Guangtao Lu, Yourong Li, Tao Wang, Wenxi Wang, & Song, G. (2017). Experimental Study on Robustness of an Eddy Current-Tuned Mass Damper. Applied Science-BASEL, 7(895). doi:10.3390/app7090895*
8. *Kirn, J., Lorkowski Thomas, & Baier Horst. (2011). Development of flexible matrix composites (FMC) for fluidic actuators in morphing systems. International Journal of Structural Integrity, 2(4), 458–473. doi:10.1108/17579861111183948*
9. *Krott, M. J., Miura, K., LaBarge, S., Christopher, D. R., Smith, E. C., & Romano, P. Q. (2015). Tube Compliance Effects on Fluidic Flexible Matrix Composite Devices for Rotorcraft Vibration Control. Paper presented at the 56th AIAA/ASCE/AHS/ASC Structures, Structural Dynamics, and Materials Conference, Kissimmee, Florida.*
10. *Krott, M. J., Miura, K., Rahn, C., & Smith, E. C. (2016). Finite Element Modeling of Fluidic Flexible Matrix Composite (F2MC) Treatments for Bending and Torsional Vibration Control. Paper presented at the 57th AIAA/ASCE/AHS/ASC Structures, Structural Dynamics, and Materials Conference San Diego, California, USA.*
11. *Lekhnitskii, S. G. (1977). Theory of Elasticity of an Anisotropic body (2nd ed.). Moscow: Mir Publishers.*
12. *Lotfi-Gaskarimahalle, A., Lioyd H. Scarborough, Christopher D. Rahn, & Edward C. Smith. (2009). Fluidic Composite Tuned Vibration Absorbers. Paper presented at the Proceedings of the ASME 2009 Conference on Smart Materials, Adaptive Structures and Intelligent Systems, Oxnard, California, USA.*
13. *Marimuthu, K. P., Kumar, C. S. C., & Prasada, H. P. T. (2018). Mathematical modelling to predict the residual stresses induced in milling process. Int. J. Mech. Prod. Eng. Res. Dev, 8(1), 423–428.*
14. *Miller, R. R. (1965). The Effects-of Frequency and Amplitude of Oscillation on the Hydrodynamic Masses of Irregular Shapes Bodies. (MS thesis), University of Rhode Island,*
15. *Miura, K., Krott, M., Smith, E., Rahn, C., & Romano, P. Q. (2015). Experimental Validation of Tailboom Vibration Control Using Fluidic Flexible Matrix Composite Tubes. Paper presented at the AHS 71st Annual Forum of the American Helicopter Society, Virginia Beach, Virginia.*
16. *Nestorović, T., Durrani, N., & Trajkov, M. (2012). Experimental model identification and vibration control of a smart cantilever beam using piezoelectric actuators and sensors. Journal of Electroceramics, 29(1), 42–55. doi:10.1007/s10832–012–9736–1*
17. *Philen, M. (2010). Tunable Modulus Structures utilizing Fluidic Flexible Matrix Composites: Analytical and Experimental InvestigationsS. Paper presented at the 51st AIAA/ASME/ASCE/AHS/ASC Structures, Structural Dynamics, and Materials Conference, Orlando, Florida.*

18. *Philen, M., Ying, S., Bakis, C. E., Wang, K. W., & Rahn, C. D. (2006). Variable Stiffness Adaptive Structures utilizing Hydraulically Pressurized Flexible Matrix Composites with Valve Control. Paper presented at the 47th AIAA/ASME/ASCE/AHS/ASC Structures, Structural Dynamics, and Materials Conference Newport, Rhode Island. http://arc.aiaa.org/doi/abs/10.2514/6.2006–2134*

19. *Sun, C. T., & Li, S. (1988). Three-Dimensional Effective Elastic Constants for Thick Laminates. Journal of Composite Materials, 22(7), 629–639. doi:10.1177/002199838802200703*

20. *Ying Shan, Michael Philen, Lotfi, A., Li, S., Bakis, C. E., Rahn, C. D., & Wang, K. W. (2009). Variable Stiffness Structures Utilizing Fluidic Flexible Matrix Composites. Journal of Intelligent Materials Systems and Structures, 20(4), 443–456. doi:10.1177/1045389X08095270*

21. *Zhu, B. (2014). Modeling, Design, and Experimental testing of Integrated Fluidic Flexible Matrix Composite Structures (Doctor of Philosophy), The Pennsylvania State University,*

22. *Zhu, B., Krott, M., Rahn, C. D., & Bakis, C. E. (2014, 2014). Experimental Characterization of a Cantilever Beam With a Fluidic Flexible Matrix Composite Vibration Treatment. Paper presented at the DETC2014-34966, Proceedings of the ASME 2014 International Design Engineering Technical Conferences & Computers and Information in Engineering Conference, Buffalo, New York, USA.*

23. *Zhu, B., Rahn, C. D., & Bakis, C. E. (2015). Fluidic flexible matrix composite damping treatment for a cantilever beam. Journal of Sound and Vibration, 340, 80–94. doi:10.1016/j.jsv.2014.11.042.*

AUTHOR PROFILE

Mr. Nazhad Ahmad Hussein is Assistant Professor in Applied Mechanics. Dean of Engineering college in Salahaddin University-Erbil. Iraq. His areas of interest in vibration, stress analysis, and smart technology. He has publications in Geometry factor determination of round specimens using fracture mechanic approaches in Al 2024-T3 (UK). Vibration Analysis of a Cracked Beam under Moving Load, (France). Effect of Heat Input and Environmental Temperature on the Welding Residual Stresses using ANSYS APDL Program Comparison with Experimental Results (Spain). Detection of Crack in Al-6063 Cantilever Beam using COMSOL Program and Experimental Work (German). The effect of gage length value in tensile test specimens on the mechanical properties of metals (Turkey). Crack Identification in Cantilever Beams Using COMSOL Program Comparison with Experimental Result (Czech). Determination of Welding Residual Stresses in Fillet Welded Joints Using ANSYS APDL Program and Comparison with Experimental Results (Malaysia). The influence of surface roughness for medium carbon steel at fatigue test on the S-N diagram (Iraq). Three-dimensional finite element simulation of arc welding process using ANSYS APDL program (Iraq). Effect of crack location and size on the natural frequencies of cracked beam using COMSOL program comparison with experimental results (Iraq). Dynamic Response of Supported Pipes Conveying Fluid (Iraq). Effect of Fiber Angles on Dynamic Response of Cantilever Composite Beams (Iraq). Theoretical, Numerical, and Experimental Analysis of Composite Double-Cracked Cantilever Beams with Various Fibers Volume Fraction and Angles (Iraq). Dynamic Response of a Cracked Composite Beam subjected to moving Load (Iraq). Study of Multi-Cracked Cantilever Composite Beams Subjected to External Moving

Load (Iraq)

Shiren Othman Muhammad has gotten her BSc degree in Mechanical Engineering (2005), MSc. in Hydraulic and Pneumatic Machines (2010), and PhD student in Applied Mechanics. She is working as Assistant Lecturer in Mechanical and Mechatronics Engineering in University of Salahaddin-Erbil. Areas of interest: Vibration, Smart structures, Control and Automation. Her publications in Modal analysis of Pneumatic two Finger Robotic hand by Finite Element Analysis and Experimental Testing (2013), Iraq. Development of Electronic-Type Finger Force Measuring System and Evaluation of Its Characteristics on Investigated Pneumatically Actuated Two Fingered Encompassing Gripper, (2014), Iraq.